Prepared for Submission to Journal of the American Ceramic Society (April 2023)

Solubility behavior and thermodynamic modeling of sodium monosulfoaluminate ("U-phase") in cementitious systems

Marie Collin ([1,2]), Dale P. Prentice ([1,2]), Ross R. Arnold ([1,2]), Kirk Ellison ([3]), Magdalena Balonis ([4]), Dante Simonetti ([2,5]), Gaurav N. Sant ([1,2,4,6])

ABSTRACT

The "U-phase", a sodium-containing (alumino-ferrite-monosubstituent) AFm phase, has been observed to form in sodium-enriched highly alkaline cementitious systems, e.g., of relevance to nuclear waste, and saline industrial brine management. But, minimal information is available of the U-phase's (e.g., solubility or thermodynamic properties) due to its limited stability and its tendency to transform into ettringite or monosulfoaluminate. Herein, the U-phase was systematically synthesized at four temperatures (5, 15, 25, and 50 °C) and fully characterized in

[1] *Laboratory for the Chemistry of Construction Materials (LC^2), Department of Civil and Environmental Engineering, University of California, Los Angeles, CA, USA*

[2] *Institute for Carbon Management, University of California, Los Angeles, CA, USA*

[3] *Electric Power Research Institute, Charlotte, NC 28262, USA*

[4] *Department of Materials Science and Engineering, University of California, Los Angeles, CA, USA*

[5] *Department of Chemical and Biomolecular Engineering, University of California, Los Angeles, CA, USA*

[6] *California Nanosystems Institute (CNSI), University of California, Los Angeles, CA, USA*

Corresponding authors: M. Collin (mariecollin03@ucla.edu) and G. Sant (Email: gsant@ucla.edu)

terms of its thermochemical properties. The average composition of the synthesized U-phase ($4CaO{\cdot}Al_2O_3{\cdot}1.85SO_3{\cdot}0.85Na_2O{\cdot}12H_2O$) deviates slightly from typical disclosures in the literature. The solubility product of the U-phase formation was measured from conditions of oversaturation. The measured thermodynamic data accurately predicted experimental observations of U-phase formation in cementitious environments. In general, it was noted that the U-phase forms, and persists (i.e., remains stable) at pH>13.7 and [Na^+] concentrations superior to 1 mol/L.

Keywords: U-phase; Sodium monosulfate; Solubility constant; Thermodynamic modeling

INTRODUCTION AND BACKGROUND

The increasing demand for high-performance cementitious materials has resulted in the development of thermodynamic databases containing hundreds of hydrated phases.(1–3) Thermodynamic modeling is a useful tool that can quickly and accurately predict the phase assemblages present at equilibrium in hydrated cementitious systems.(4,3,5,1,6) For this reason, it has been utilized in multiple applications, including civil engineering,(7,8) nuclear waste management,(2,9) and/or liquid wastewater stabilization.(10–12) While many of the common cementitious (e.g., Ordinary Portland Cement, OPC) hydration products can be accurately predicted,(1,4,6,13,14) modeling of uncommon systems remains challenging since the measured thermodynamic properties of less prominent phases may not be available in current databases.

Alkali- and sulfate-enriched containing cementitious systems are an example of uncommon systems. These systems are of interest in specialty areas such as: (a) stabilizing nuclear wastes with a high Na_2SO_4 content,(15) (b) stabilization of hyperalkaline wastewaters (e.g., flue gas desulfurization wastewater, contaminated groundwater, produced water, etc.) that is often solidified/stabilized (S&S) in cementitious matrices,(16,17) and (c) alkali-activated slags that are an alternative cementation solution (to OPC).(3,18,19) In each of these cases, the cementitious system may contain a high level of sodium and sulfate that can promote the formation of the "U-phase", a sodium-containing AFm phase that has been identified previously in high Na_2SO_4 hydrated systems.(15,20) More commonly, the hydrated Al_2O_3-Fe_2O_3-mono- (AFm, e.g., monosulfate) and -tri- (AFt, e.g., ettringite) phases are observed in cementitious systems.(21–27) The domain of stability of the mono- and tri- compounds, in addition to the calcium-silicate-hydrates (C-S-H), hydrogarnets (e.g., katoite), hydrotalcite-like phases, etc., is well established.(22) But, since the U-phase's formation is far less common, less is known about the properties of this compound, and the conditions of its coexistence with other common cementitious phases.

The U-phase was first analyzed by Dosch et *al*.,(20) who proposed a nominal composition of $4CaO{\cdot}0.9Al_2O_3{\cdot}1.1SO_3{\cdot}0.5Na_2O{\cdot}16H_2O$. Both the U-phase's composition and morphology are related to monosulfate ($4CaO{\cdot}Al_2O_3{\cdot}SO_3{\cdot}12H_2O$),(15,20) yet the U-phase has only been observed to form in highly alkaline environments.(28–32) Despite being observed in multiple Na_2SO_4-containing systems,(15,20,28,29,31,32) there is limited proposed U-phase's solubility data, and the values varies by as much as 10 log K_{so} units from one study to the other (e.g.,

log K_{so} = 78.96 from Champenois et *al.*(33), log K_{so} = 68.56 from Kajio et *al*.(34) as reported by Chuang et *al*.(35)). This is because, for example, when placed in contact with water, the U-phase rapidly transforms into ettringite, which prohibits accurate solubility measurements from undersaturation.(20) Previous studies have often excluded the U-phase from thermodynamic modeling (of phase assemblages) when using GEM-Selektor (GEMS)(36) and PHREEQC(37), and only a couple of studies implemented it in their modeling using PHREEQC only.(33,35) However, adding this phase to thermodynamic databases is becoming increasingly relevant. For example, zero-liquid discharge (ZLD) guidelines in the U.S. are requiring reductions in the volume of liquid waste produced during industrial operations.(38–42) Liquid concentration steps result in the production of hypersaline solutions that require S&S with a cementitious material before being safely landfilled.(38–42) The concentrated wastewaters used herein can feature high Na_2SO_4 contents. It is thus necessary to assess the propensity of the U-phase to form preferentially over other AFm or AFt phases of interest to ensure robust S&S. Furthermore, the U-phase's formation or destabilization has been suggested to damage the cementitious solid due to shrinkage or expansion mechanisms that can result in cracking.(15,30,31,43) Therefore, it is necessary to understand and predict the conditions under which U-phase formation can occur.

To obtain a self-consistent set of solubility data, the U-phase was synthesized at four different temperatures (5, 15, 25, and 50 °C), and the solid and solution compositions were fully assessed by a multi-method characterization approach. The results were used to establish the solubility constant (K_{so}) and thermodynamic data (molar volume, enthalpy, entropy, heat capacity)

necessary to model the formation of the U-phase. The resulting thermodynamic dataset accurately reproduces observations of U-phase formation in experimental systems.

MATERIAL AND METHODS

U-phase synthesis: The U-phase was synthesized following the protocol of Li et *al.*,(44) wherein 0.4 M of metal Al was carefully dissolved in 1 L of a 1 M NaOH solution, then reacted with 0.5 mol of $Ca(OH)_2$ and 0.5 mol of Na_2SO_4 (both sieved through a 100 µm sieve prior to the synthesis). The slurry was agitated at room temperature for 7 days, then divided into 12 hermetically sealed plastic containers. Triplicate samples were held isothermally at four temperatures (5, 15, 25, and 50 °C) and aged under agitation for a month. Following one-month of aging, the pH of the solution was measured using a Rapid RH® Digital pH Meter. The solution was sampled and passed through a 0.2 µm filter to separate the solid from the solution.

Na and Al elemental concentrations were measured by ICP-OES using a Perkin Elmer Avio 200 instrument, and Ca elemental concentration was measured by ICP-MS using a Perkin Elmer NexION 2000 instrument. In both cases, the filtered solution was stabilized in a 5 vol % nitric acid matrix, and three spectra were collected per sample and converted to molar concentration units from calibration curves prepared with standard solutions (Inorganic Ventures, 1000 ppm). SO_4^{2-} concentrations were measured using a method analogous to ASTM D516 wherein SO_4^{2-} is reacted with barium to form (very slightly soluble) barium sulfate. The turbidity of the resulting solution was measured using a Go Direct® SpectroVis® Plus Spectrophotometer and converted

to molar concentration units via a calibration curve prepared with a standard SO_4^{2-}solution (Inorganic Ventures 1000 ppm).

The solids synthesized at 5, 15, 25, and 50 °C were retrieved by vacuum filtration and immediately characterized to minimize the potential for carbonation or phase destabilization. A small fraction of each solid was retrieved and immediately dissolved in deionized water (DIW; 5 mg of solid in 50 mL of DIW, i.e., 1:10000 solid to liquid ratio). The resulting solution was analyzed following the protocol detailed above to assess the solid composition.

Thermogravimetric analysis: Thermogravimetric analysis (TGA) was performed using a Perkin Elmer STA 6000 under a flow of ultrapure nitrogen in aluminum oxide crucibles. A heating ramp of 10 °C/min was used between 35 and 950 °C, after 5 min equilibration at 35 °C. The thermogravimetric mass loss (TG) and the derivative mass loss (DTG) were both used to quantify the amount of physically sorbed and chemically-bonded water in the U-phase.(45,46)

X-Ray diffraction: XRD analysis was performed using a PANalytical X'Pertpro diffractometer (θ-θ configuration, CuKα radiation, λ = 1.54 Å) on powdered samples. In general, due to the small amount of sample available, the powdered samples were dispersed on a zero-background plate and directly analyzed. Scans were acquired between 5° and 70° with a step-size of 0.02° using a scientific X'Celerator 2 detector. The unit cell parameters of the four crystalline samples were refined using CELREF.(47)

Infrared spectroscopy: Solid-state attenuated total reflection Fourier-transform infrared spectroscopy (ATR-FTIR) was performed using a Spectrum Two FT-IR Spectrometer (Perkin Elmer). The powdered samples were pressed using around 90 N of force onto a diamond/ZnSe composite crystal to ensure adequate contact and generate total internal reflection. The spectra reported herein were obtained by averaging 4 scans over the wavenumber range of 4000-to-400 cm^{-1} at a resolution of 1 cm^{-1}.

Scanning electron microscopy with energy dispersive X-ray spectroscopy: SEM-EDS analysis was performed using a Phenom™ XL G2 Desktop SEM operated at 15 keV. Four areas were analyzed per sample (at a magnification of 1000x) using a solid-state ultrafast silicon detector to ensure accurate measurements and limit sample damage, particularly Na-migration under the e^--beam.

Helium pycnometry: The solid's density was measured using helium pycnometry (AccuPyc II 1340, Micrometrics). Around 0.5 g of sample was used for each measurement. A cyclical helium flush procedure was set to repeat until a stable vacuum pressure (i.e., degas stage) was achieved, at which point ten data points were collected via additional helium purges.

Thermodynamic modeling: Thermodynamic modeling was carried out using GEM-Selektor v.3.6 (GEMS)(48,49) which incorporates the slop98.dat and Cemdata18 thermodynamic databases.(1,50–52) Property inputs from these databases are used to calculate the activities of aqueous species, to estimate the solubility constants, and estimate stable phase assemblages. Following the provision of new thermodynamic data applicable to the U-phase, these

databases, and the GEMS platform were additionally used to examine the tendency of the U-phase to form in sulfate-enriched, alkaline cementitious systems. To represent the non-ideality of the solutions, the ion activity coefficients were calculated using the Truesdell-Jones extension to the Debye-Hückel equation:(53)

$$\log_{10}\gamma_i = \frac{-A_\gamma z_i^2\sqrt{I}}{1 + \dot{a}B_\gamma\sqrt{I}} + b_\gamma I + \log_{10}\frac{X_{jw}}{X_w} \qquad \text{Equation 1}$$

where, γ_i is the activity coefficient and z_i the charge of the i^{th} aqueous species, A_γ and B_γ are temperature and pressure dependent coefficients, X_{jw} is the molar quantity of water, X_w is the total molar amount of the aqueous phase, and I is the molal ionic strength (≤2 mol/L). A common ion size parameter ($\dot{a}$ = 3.72 Å) and a short-range interaction parameter (B_γ = 0.64 kg/mol) were used, treating NaCl as the background electrolyte.(53,54)

RESULTS AND DISCUSSION

U-phase solid characterization: The solids synthesized at 5, 15, 25, and 50 °C were characterized to assess their: (a) crystal structure, (b) morphology, (c) composition, and (d) water content. The XRD patterns of the solids confirm that all four phases are phase pure, crystalline U-phase (Figure 1a). No significant differences were observed between the solids' diffraction pattern across the different synthesis temperatures. The peak positions and intensity are in agreement with the literature,*(20,31,44)* and correspond to the typical hexagonal layered AFm structure. Similarly, the IR spectra (Figure 1b) are consistent with that expected for SO_4^{2-}-containing AFm or AFt phases: Ca-O and Al-O stretching bands are observed below 1000 cm^{-1}, and an intense SO_4^{2-} vibration band is observed at 1100 cm^{-1}. The SO_4^{2-} vibration band position is lower than that of monosulfate (1150 cm^{-1}) and ettringite (1115 cm^{-1}).*(55)* A small CO_3^{2-} signal is observed between 1300 and 1500 cm^{-1}, likely due to surficial carbonation of the sample during drying. Interstitial molecular H_2O bending vibrations produce a small signal around 1650 cm^{-1}, and interstitial molecular H_2O stretching vibrations cause a broad signal between 2900 and 3700 cm^{-1}. Additionally, two peaks at 3545 and 3670 cm^{-1} can be attributed to hydroxyl groups – Al-OH and Ca-OH respectively – similar to that observed in monosulfate or ettringite.*(55,56)*

TGA analysis shows three mass loss regions attributed to water's evaporation between 50-130, 130-230, and 230-350 °C (Figure 1c), similar to that observed for monosulfate.(45) The first two mass losses are attributed to molecular water removal, while the third mass loss represents dehydroxylation.(45) The total amount of water is consistent with the observations of Dosch et *al*.(20) of multiple hydration states for the U-phase ranging from 8-to-16 (total) water

molecules. On average, the U-phase synthesized herein features 12 water molecules; i.e., similar to monosulfate.(45) The total amount of water remains unchanged across synthesis temperatures, but the ratio between interstitial water molecules and hydroxyl groups varies, with an increasing hydroxyl content observed with increasing temperature (Table 1). Under water saturated conditions, temperature slightly (if at all), affects the total amount of water present,(57) although it can affect the distribution of water, i.e., the molecular water/hydroxyl ratio of AFm phases. The samples showed minimal signs of surficial carbonation (<3 mass %) that likely occurred during drying, which is not considered in the analysis of the solid phase composition that follows.

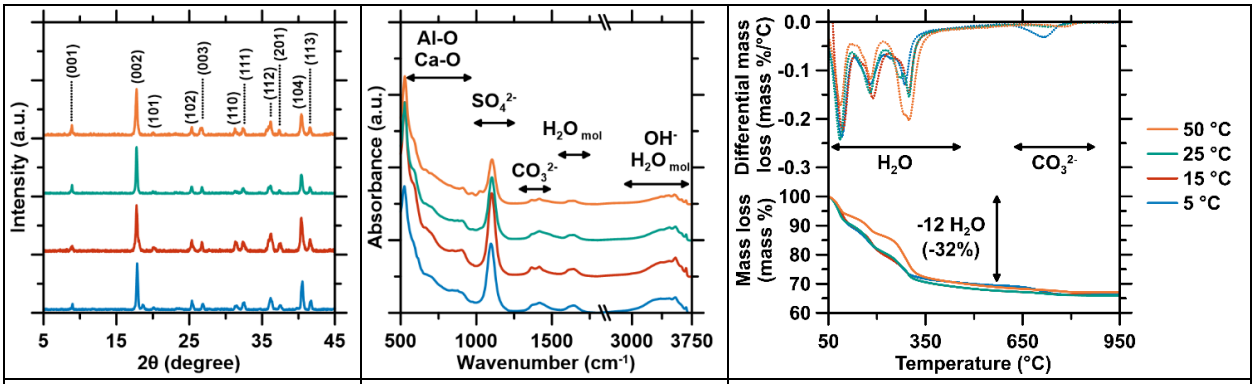

(a) **(b)** **(c)**

Figure 1. The solid-phase characterization of the U-phase synthesized at 5, 15, 25, and 50 °C using **(a)** XRD, **(b)** IR spectroscopy, and **(c)** TGA.

Table 1. The water content of the U-phase as estimated via TGA analysis and the density of the compound as synthesized at 5, 15, 25, and 50 °C.

Synthesis Temperature	Water content (mass %)			
	H_2O molecular (Region 1)	H_2O molecular (Region 2)	H_2O hydroxyl groups (Region 3)	Total water mass loss
5 °C	11.0	9.4	10.0	30.5
15 °C	10.5	10.1	11.6	32.2
25 °C	10.4	9.4	12.5	32.2
50 °C	7.3	6.7	16.9	31.0

The U-phase's morphology is similar across synthesis temperature: the U-phase forms as thin hexagonal crystals (Figure 2a) similar to AFm-phases such as monosulfate.(20,29,58) Compositional analysis of the samples – as assessed by solid digestion – confirms the presence of Na in the solid, which reinforces the status of the U-phase as a sodium-containing AFm phase (Figure 2b). A similar composition is observed across synthesis temperatures. Interestingly, the present compositions differ from the composition proposed by Dosch et *al*.(20) – $4CaO{\cdot}0.9Al_2O_3{\cdot}1.1SO_3{\cdot}0.5Na_2O{\cdot}16H_2O$ – as follows: Lower Ca (-4.6 at % on average) and Al (-0.8 at % on average) contents, and higher SO_4^{2-} (+2.0 at % on average) and Na (+2.2 at % on average) contents are observed. The composition determined herein is closer to the composition proposed by Kajio et *al*.(34) (as reported by Chuang et *al*.(35)): $4CaO{\cdot}Al_2O_3{\cdot}1.5SO_3{\cdot}0.75Na_2O{\cdot}16H_2O$. The solid's composition was also calculated from the composition of the "mother liquor" from which the solid forms, and by SEM-EDS for further validation. All three methods give similar results (Figure S1). SEM-EDS underestimates the amount of Na in the U-phase likely due to Na migration under the 15 keV beam.(59) In contrast, the leachate analysis likely overestimates the amount of Na in the U-phase: this method of calculation has the highest uncertainty due to the abundance of Na – that is initially present in solution from Na_2SO_4 and NaOH – remaining in solution after solid precipitation. Nevertheless, the agreement between the three methods validates the compositions obtained.

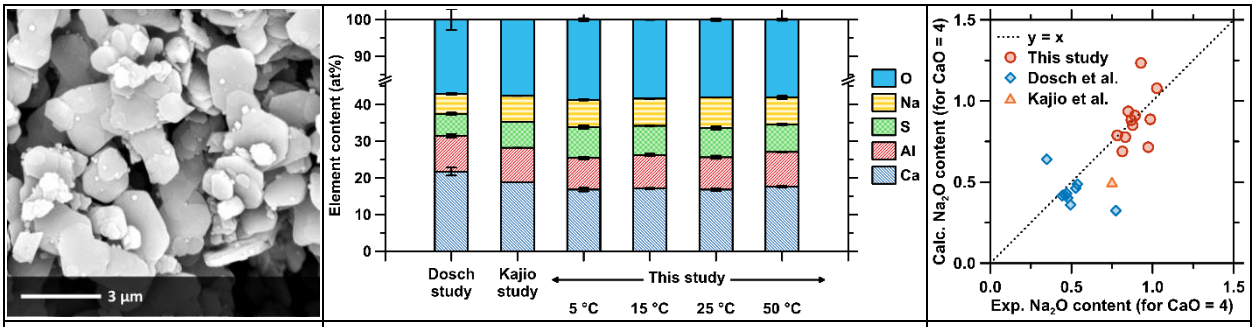

(a) **(b)** **(c)**

Figure 2. (a) A representative SEM image (sample synthesized at 50 °C) shows the U-phase in the form of thin hexagonal crystals, a morphology similar to that of SO_4-AFm. **(b)** The average composition of the samples synthesized at 5, 15, and 25 °C, compared with the compositions from the literature.(20,35,44) The error bars show the standard deviation of triplicate measurements (this study), or from 9 measurements (Dosch et *al.*(20)). **(c)** The comparison between the experimental and calculated Na_2O content (see Equation 2) of the samples synthesized herein, and the samples synthesized by Dosch et *al.,*(20) and by Kajio et *al*.(34) as reported by Chuang et *al*.(35).

Despite the variations in compositions observed in the literature,(20,35,44) the compositions calculated herein are consistent with Equation 2 as proposed by Dosch et *al*.:(20)

$$4CaO{\cdot}(1-x)Al_2O_3{\cdot}(1+y)SO_3{\cdot}(3x+y)Na_2O \qquad \text{Equation 2}$$

Particularly, the solids synthesized herein display, on average, x = 0 (i.e., no Al deficit in the lattice), while the "y-value" (i.e., the excess of SO_4) results from Na_2SO_4 incorporation in the interlayer positions. A good agreement between the calculated and experimental Na_2O content is observed (Figure 2c), as also observed by Dosch et *al*.(20), and by Kajio et *al*.(34) as reported by Chuang et *al*.(35) This further confirms that the U-phase's composition represents a solid-solution that is strongly affected by the initial solution's composition.(20)

The unit cell dimensions of the U-phase (see Table 2) calculated from X-ray reflections are similar to literature observations.(20,44) This suggests that the U-phase's crystallography

remains largely unaffected by nominal difference in composition compared with the study of Dosch et *al.*(20) Unlike composition, the density of the solids (Table 2) shows slight variation as a function of temperature of synthesis, with a higher value measured at 50 °C, with all values being ~10% higher than literature records.(44) These differences likely stem from variations in the water content. Even "gentle" drying (e.g., short drying at ambient conditions following vacuum filtration) prior to density measurements can strongly affect an AFm's degree of hydration if the relative humidity is not controlled.(20) Although no hydration values are provided by Li et *al*.,(44) and the water content measured herein is similar across synthesis temperatures (Table 1), it is still likely that the U-phase herein may have been slightly dehydrated; which would explain the marginally higher density – in spite of the consistency of values of the unit cell dimensions. This may suggest a departure from Vegard's law (i.e., unlike typical AFm compounds) such that up to some moisture content inferior to saturation, the unit cell parameters show no change with modest changes in the moisture content.(60)

Table 2. The density and unit cell parameters of the four hexagonal (a = b ≠ c [Å, angstroms], α = β = 90 °, γ = 180 °) U-phase samples synthesized at 5, 15, 25, and 50 °C. Also noted, for comparison, are unit cell parameters from the literature for a freshly prepared sample.(20,44)

	***a*-parameter (Å)**		***c*-parameter (Å)**		**Density (g/cm^3)**	
Phase	**This study**	**Literature**	**This study**	**Literature**	**This study**	**Literature**
5 °C	5.75	-	10.00	-	2.12	
15 °C	5.75	-	10.00	-	2.08	
25 °C	5.75	5.74-5.76	10.00	10.00	2.14	1.95
50 °C	5.75	-	10.00	-	2.21	

The average U-phase density and U-phase composition as selected for the thermodynamic modeling assessment are detailed in Table 3.

Table 3. The average composition and density of the U-phase as used in thermodynamic modeling, and database development.	
Composition	**Density (g/cm^3)**
$4.0CaO{\cdot}1.0Al_2O_3{\cdot}0.85Na_2O{\cdot}1.85SO_3{\cdot}12H_2O$	2.11

U-phase solubility measurement: Solubility measurements can be carried out in two ways: (a) from undersaturation, wherein a solid is dissolved into a liquid – generally deionized water (DIW) – until saturation with respect to the dissolving phase is reached, and (b) from oversaturation, wherein the solid is precipitated from a supersaturated solution. Analysis from undersaturation is not an option for the U-phase since it is highly unstable in DIW. For this reason, analysis from oversaturation was carried out. The composition – i.e., the pH of the solution and Ca, Na, Al, and SO_4^{2-} concentrations – of the "mother liquor" (the solution from which the solid forms) was analyzed. Three replicate measurements were carried out at each temperature (Table S1, Figure 3a and b). Overall, the concentrations remained similar across the temperature range studied (Figure 3a). A slight decrease in the Al concentration was observed at 50 °C that did not result in meaningful changes in the solid composition (Figure 2b). Of note, no other phases – such as hydrogarnet that is known to be more stable at higher temperatures*(61)* – were observed even at 50 °C. The solution's pH decreased as a function of temperature in a linear manner (Figure 3b).

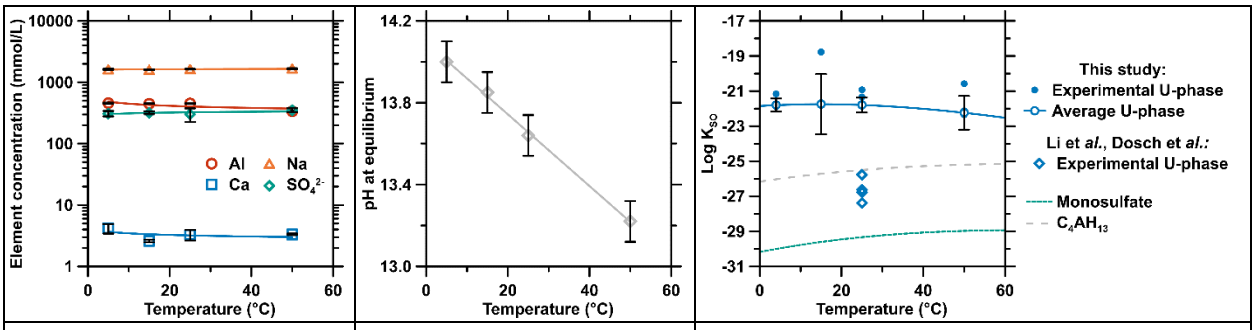

Figure 3. The composition of the "mother liquor" from which the solid forms determined experimentally at 5, 15, 25 and 50 °C: **(a)** Al, Na, Ca, and SO_4^{2-} concentration (the error bars show the standard deviation of triplicate measurements), and **(b)** the pH of the leachate (the error bars represent the uncertainty of the instrument – ± 0.1 pH unit). **(c)** The calculated solubility constants (logK_{so}) of the synthetic phases (plotted as symbols, with the error bars showing the standard deviation of triplicate measurements) as a function of temperature. The experimental data are fitted by Equation 9. The U-phase solubility is then compared to U-phase's solubility constants from the literature,(43) and to similar AFm phases.(23,62)

The solubility constant (K_{so}, unitless) of the U-phase was calculated assuming a congruent reaction (Equation 3), using the reaction stoichiometry in the solubility calculation (Equation 4) as follows:

$$Ca_4Al_2Na_{1.7}(SO_4)_{1.85}(OH)_{12} \cdot 6H_2O \rightarrow 4(Ca^{2+}) + 2(AlO_2^{-}) + 1.85(SO_4^{2-}) + 1.7(Na^{+}) + 4(OH^{-}) + 10(H_2O) \quad \text{Equation 3}$$

$$K_{so} = a_{Ca^{2+}}^{4} \cdot a_{AlO_2^-}^{2} \cdot a_{SO_4^{2-}}^{1.85} \cdot a_{Na^+}^{1.7} \cdot a_{OH^-}^{4} \cdot a_{H_2O}^{10} \quad \text{Equation 4}$$

where, K_{SO} is the solubility constant and a_i^x is the activity of a given ionic species with stoichiometric coefficient x. For example, $a_{H_2O}^{10}$ is the activity of water with stoichiometric coefficient 10. The activities and speciation of the aqueous components were calculated using GEMS. The calculated solubility constant at 25 °C varies slightly from that calculated by Li et *al*.(43) from the solution dataset of Dosch et *al*.(20) (Figure 3c). For the Li et *al*.(43) system, the

U-phase formed alongside other hydrated phases (e.g., sodium sulfate, monocarboaluminate, gibbsite, and hydrogarnet), and the calcium and OH^- concentrations were estimated using an iterative method combining the solubility constant of C_4AH_n and the experimental Al_2O_3 concentration associated to the electroneutrality equation. As such, their calculated log K_{so} as displayed in Figure 3c would likely result in a higher uncertainty than that calculated in this study, as it is calculated from a mixed-phase system with estimated values. However, the differences observed between log K_{so} reported in the literature and the value reported herein may also reflect differences in the solubility of the U-phase solid solution. More work is thus necessary to assess the full range of solubility of the U-phase. The average solubility constant of the U-phase calculated here decreases slightly with increasing temperature (Figure 3c). This trend is consistent with that of other AFm and AFt phases.(23,62) The solubility constant of the U-phase is larger (i.e., it is a less negative number) than other AFm and AFt phases. This is consistent with previous observations that the U-phase is easily destabilized into monosulfate or ettringite via the following transformation reactions:(20)

$$\text{Ettringite} \underset{H_2O}{\overset{NaOH}{\rightleftarrows}} \text{U-phase} \xrightarrow[Ca(OH)_2]{-NaOH} \text{Monosulfate} \qquad \text{Equation 5}$$

Thermodynamic modeling of U-phase formation: The solubility constant of the U-phase was used in combination with the chemical potentials of the aqueous species to determine the Gibbs energy of formation at standard conditions ($\Delta_f G^0_{298}$) using Equation 6:(62,63)

$$\Delta_r G^0_{298} = \sum_i v_i \Delta_f G^0_T = -RT\ln(K_{sp}) \quad \text{Equation 6}$$

where, $\Delta_r G^0_{298}$ is the Gibbs free energy of reaction at 298 K, v_i is the stoichiometric reaction coefficient, $\Delta_f G^0_T$ is the Gibbs free energy of formation of the ionic species detailed in Equation 4 (refer to Table S2 for the values)(52,64), *R* is the ideal gas constant (8.314 J/mol/K), and *T* is the temperature in K. The standard absolute isobaric heat capacity (Cp°_{298}) was estimated following the reference reaction (refer to Table S2 for the reference heat capacity values)(50,51,64–70):

$$\mathrm{Ca_4Al_2(SO_4)_1(OH)_{12}\cdot 6H_2O\ (Monosulfate)} + 0.85\mathrm{Na_2(SO_4)\ (Thenardite)} \rightarrow \mathrm{Ca_4Al_2Na_{1.7}(SO_4)_{1.85}(OH)_{12}\cdot 6H_2O\ (U-phase)} \quad \text{Equation 7}$$

The enthalpy of reaction ($\Delta_r H^0_{T_0}$) and the entropy of reaction ($\Delta_r S^0_{T_0}$) are interdependent via the Gibbs free energy:

$$\Delta G = \Delta H - T\Delta S \quad \text{Equation 8}$$

The entropy of reaction is fitted from the solubility constants of the U-phase using the three-terms temperature extrapolation:(62)

$$\log K_T = A_0 + A_2 T^{-1} + A_3 \ln T \quad \text{Equation 9}$$

$$A_0 = \frac{0.4343}{R}.\left[\Delta_r S^0_{T_0} - \Delta_r Cp^0_{T_0}.(1+\ln T_0)\right] \quad \text{Equation 10}$$

$$A_2 = \frac{0.4343}{R}.\left[\Delta_r H^0_{T_0} - \Delta_r Cp^0_{T_0}.T_0\right] \quad \text{Equation 11}$$

$$A_3 = \frac{0.4343}{R}.\Delta_r Cp^0_{T_0} \quad \text{Equation 12}$$

The calculated thermodynamic properties are displayed in Table 4. Note that the entropy value is close to the value inferred from Equation 7 (918.7 J/mol/K). The entropy and heat capacity values displayed in Table 4 are also consistent with the trend observed for other phases from the slop98.dat, Cemdata18, and Zeo19 thermodynamic databases(1,5,50–52,71), when considering the volume-based thermodynamics approach (Figure S2).(72,73)

Table 4. The thermodynamic properties of the U-phase used in the modeling: V^0 – molar volume; K_{S0} – thermodynamic equilibrium constant at T_o = 298 K; $\Delta_f G°$ – standard molar Gibbs energy of formation at T_o = 298 K; $\Delta_f H°$ – standard molar enthalpy at T_o = 298 K; $S°$ – standard molar entropy at T_o = 298 K; $C°_p$ – heat capacity at T_o = 298 K.

V°	**log K_{so}**	$\Delta_f G^\circ_{298}$	$\Delta_f H^\circ_{298}$	S°_{298}	$C^\circ p_{298}$
(cm^3/mol)		(kJ/mol)	(kJ/mol)	(J/mol/K)	(J/mol/K)
352.25	-21.79 ± 3.27	-8873.87 ± 1331.08	-9878.55 ± 1481.78	972.15 ± 145.83	1003.70

The thermodynamic properties displayed in Table 4 only encompass the composition synthesized and studied herein. It does not include additional compositions and solubility results previously reported.(20,35,43) It is also fully limited to the sodium-based U-phase, and exclude the potassium-based U-phase that has been observed to form in high K_2SO_4 containing systems.(32) The tendency of the proposed U-phase to form and persist was thus examined and compared for two experimental systems from the literature where: (a) the U-phase was observed to form, and (b) was quantified.(31,32) First, thermodynamic modeling shows a good ability to reproduce U-phase formation in a system composed of White Portland Cement (WPC)

hydrated with a Na_2SO_4 solution (1.05 mol/L, s/l = 1.67, Figure 4a and b). The modeling assumed that the clinker minerals react at a similar rate, and following their mass abundance (56.77 mass % alite, 15.03 mass % belite, 3.98 mass % tricalcium aluminate, and 0.01 mass % ferrite). Practically however, the rate of reaction of the clinker minerals is known to differ.(4,74–76) In general, the modeled quantities of hydrated phases are similar to experimental assessments. An exception is thenardite which is not observed to form in the modeled system. Thenardite features a stability that is similar to that of ettringite and the U-phase in the system studied herein. This is likely the reason why it is not observed to form in the model system. Second, thermodynamic modeling also correctly recreates the experimental results for a C_3A-$CaSO_4{\cdot}2H_2O$ system reacted with a Na_2SO_4 solution (0.67 mol/L, s/l = 1.67, Figure 4c and d). The major difference observed is the “gel phases” that are postulated to form in the experimental system. The existence of the gel phases was postulated based on mass balance analysis considering the reaction rates of the reactants and the quantities of hydrated phases formed.(32) However no compositional information is provided, meaning these phases could not be included in the modeling. While it is indeed possible that the gel phases are an intermediate/metastable state that precludes crystalline hydrate formation, they cannot be considered in an equilibrium state model. Despite this issue, the modeling properly reproduces the transition from ettringite to the U-phase and monosulfate as observed experimentally after 12 hours of hydration.

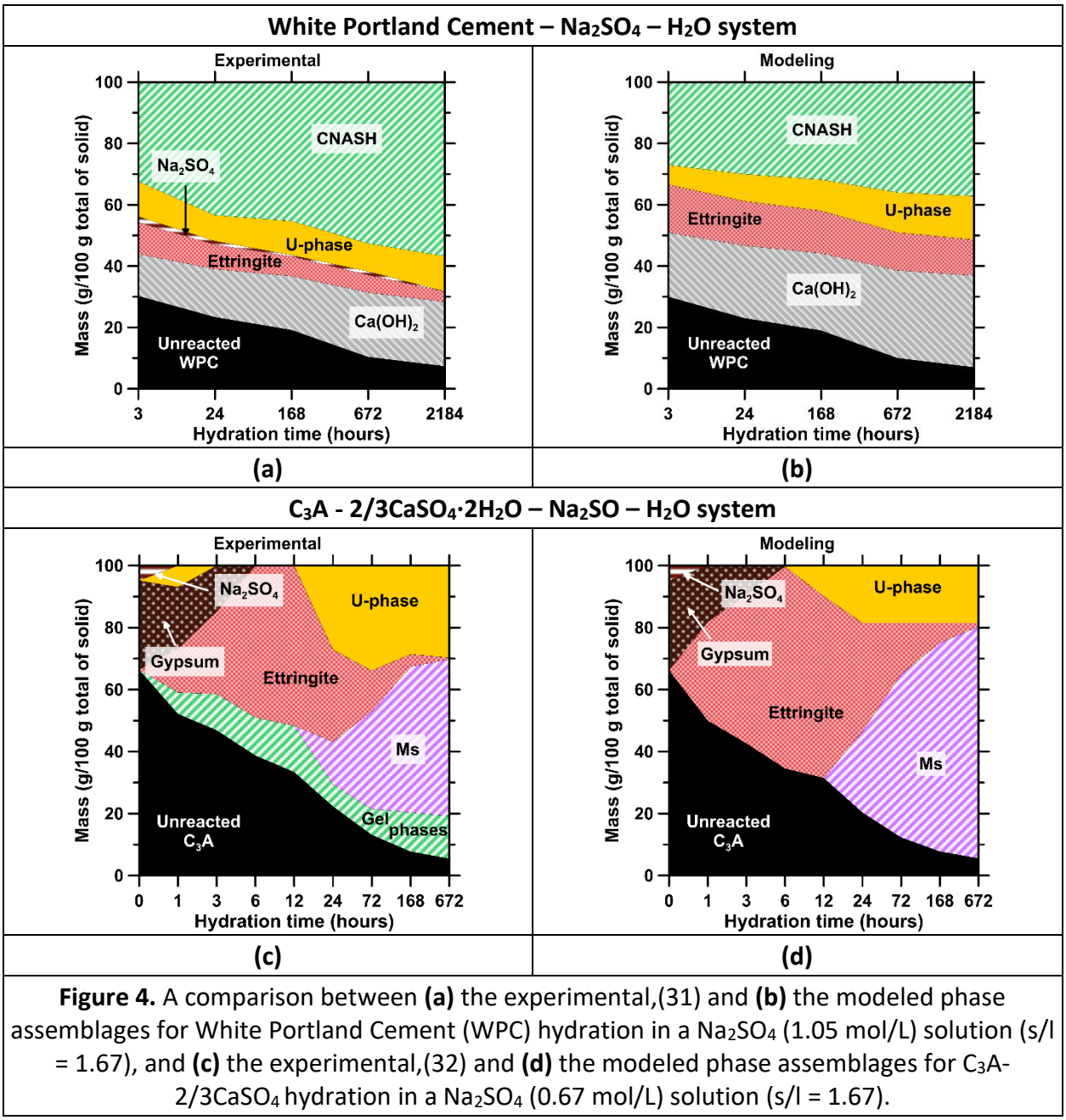

Figure 4. A comparison between **(a)** the experimental,(31) and **(b)** the modeled phase assemblages for White Portland Cement (WPC) hydration in a Na_2SO_4 (1.05 mol/L) solution (s/l = 1.67), and **(c)** the experimental,(32) and **(d)** the modeled phase assemblages for C_3A-2/3$CaSO_4$ hydration in a Na_2SO_4 (0.67 mol/L) solution (s/l = 1.67).

The rather good agreement observed between experimental and modeled phase assemblages herein may in fact suggest that the U-phase model proposed herein may not encompass the entire U-phase solid solution. Regardless, the current model is sufficient to assess the parameters that affect the U-phase's domains of stability. Towards this end, first, the phase

assemblage formed at equilibrium is examined for C_3A reacted with excess portlandite as a function of increasing $NaOH/Al_2O_3$ ratio and increasing SO_3/Al_2O_3 ratio, at a fixed solid-to-liquid (s/l, mass basis) ratio of 0.1 (Figure 5a). It is observed that high $NaOH/Al_2O_3$ ratios are necessary for the U-phase to form. This is consistent with experimental observations: the U-phase typically forms only in highly alkaline environments. Further, increasing the $NaOH/Al_2O_3$ ratio progressively diminishes the abundance of other phases (ettringite, monosulfate, and/or katoite) at the expense of the U-phase until only the U-phase persists. These results are consistent with Equation 5 that shows ettringite's destabilization into U-phase with increasing alkalinity with a similar destabilization being applicable for monosulfate, albeit at lower SO_3/Al_2O_3 ratios. The U-phase's formation is predominantly dependent on pH (NaOH concentration). For example, while no U-phase formation is observed at a s/l = 0.1 where $SO_3/Al_2O_3 = 1.5$ and $NaOH/Al_2O_3 = 0.5$, increasing (only) NaOH concentration rapidly induces the formation of the U-phase (Figure 5b). The U-phase begins forming at an initial NaOH concentration of 1 mol/L and persists thereafter. The pH at these conditions (pH 13.7) is high enough to promote the stability of the U-phase over ettringite, and is consistent with Figure 5a which suggests the formation of the U-phase for pH's over 13.7.

Finally, it should be noted that the formation of the U-phase has been noted to be detrimental to nuclear waste stabilization and could, in fact, also be detrimental for brine encapsulation. The U-phase phase, as noted previously, is extremely unstable: if exposed to water (e.g., ground water, rain, etc.), it may revert to ettringite (Equation 5 and Figure 5b). The resulting volume expansion is significant (Figure 5c), and may cause severe cracking of the solid matrix,

as observed elsewhere.(30,31) This would compromise the integrity of the solid matrix, highlighting a need to prevent the initial formation of the U-phase and/or limit the contact of a U-phase containing matrix with a water stream. In the case of brine encapsulation, U-phase formation can be avoided by controlling the brine composition. For example, the production of a liquid with high sulfate and sodium content should be avoided to prevent the U-phase formation and ensure that the produced solid matrix will remain physically and chemically stable over time.

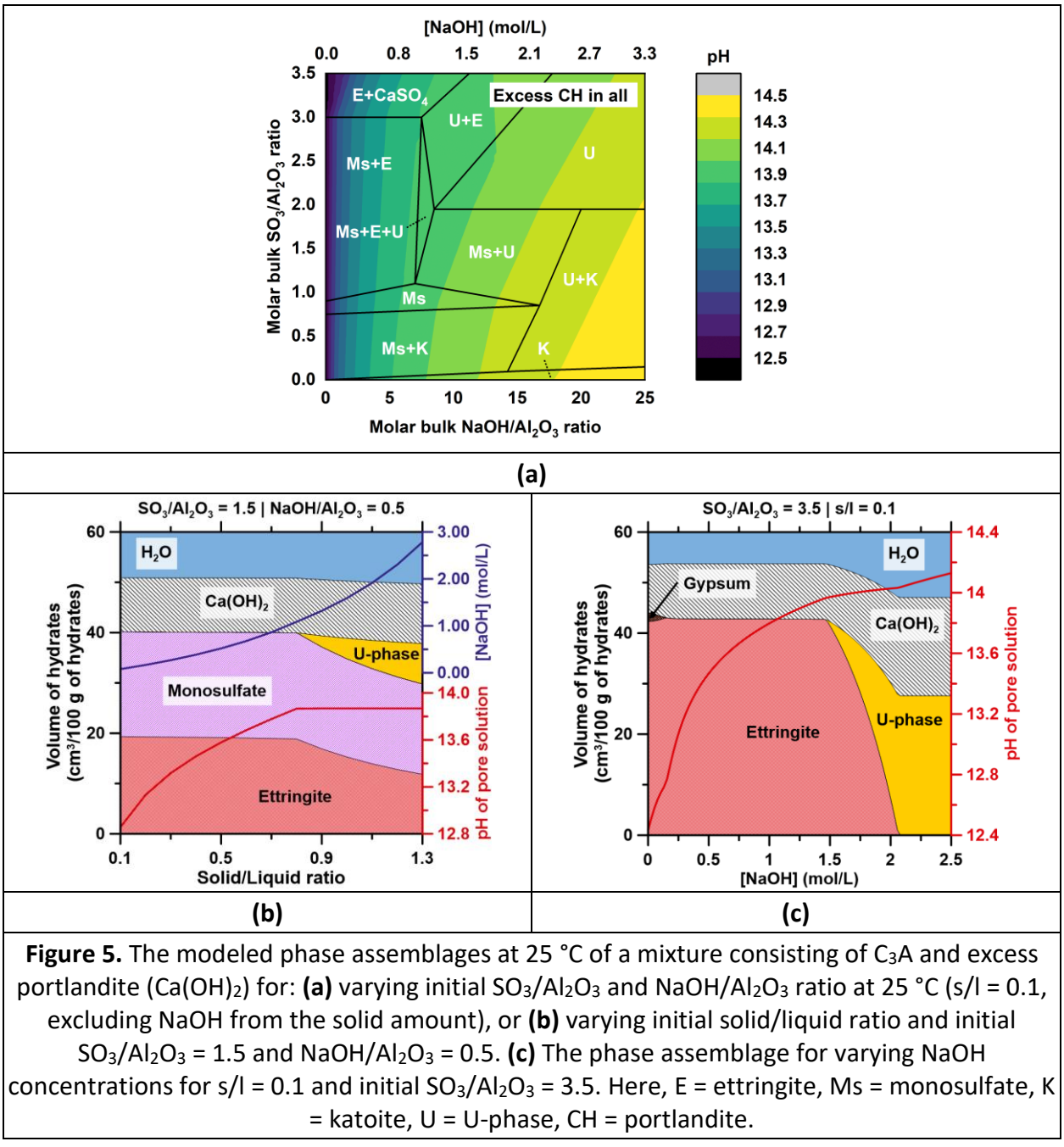

Figure 5. The modeled phase assemblages at 25 °C of a mixture consisting of C_3A and excess portlandite ($Ca(OH)_2$) for: **(a)** varying initial SO_3/Al_2O_3 and $NaOH/Al_2O_3$ ratio at 25 °C (s/l = 0.1, excluding NaOH from the solid amount), or **(b)** varying initial solid/liquid ratio and initial SO_3/Al_2O_3 = 1.5 and $NaOH/Al_2O_3$ = 0.5. **(c)** The phase assemblage for varying NaOH concentrations for s/l = 0.1 and initial SO_3/Al_2O_3 = 3.5. Here, E = ettringite, Ms = monosulfate, K = katoite, U = U-phase, CH = portlandite.

SUMMARY AND CONCLUSIONS

The U-phase was synthesized at four different temperatures (5, 15, 25, and 50 °C). The composition and structure of the solids were fully characterized using IR spectroscopy, XRD, TGA, SEM-EDS, and solution phase compositions. The results indicate the similarity of

composition and morphology of the U-phase and monosulfate. The average composition of the U-phase proposed herein: $4CaO{\cdot}Al_2O_3{\cdot}1.85SO_3{\cdot}0.85Na_2O{\cdot}12H_2O$ is slightly dissimilar from the compositions previously reported in the literature: $4CaO{\cdot}0.9Al_2O_3{\cdot}1.1SO_3{\cdot}0.5Na_2O{\cdot}16H_2O$ and $4CaO{\cdot}Al_2O_3{\cdot}1.5SO_3{\cdot}0.75Na_2O{\cdot}16H_2O$. This suggests that the composition of the U-phase may: (a) depend on the starting conditions, and solution compositions, and (b) represent a solid solution which remains to be fully defined. From oversaturation, the solubility constant of the U-phase was estimated, and thereafter used to estimate its thermodynamic properties (molar volume, enthalpy, entropy, heat capacity). The resulting thermodynamic dataset was able to correctly reproduce the equilibrium phase assemblage of cementitious systems where the U-phase was observed to form and persist. Phase diagrams constructed using these original thermodynamic data indicate that U-phase formation is strongly dependent on the NaOH concentration, i.e., the pH of the system. It is observed to form mostly at high NaOH concentration (typically greater than 1 mol/L) and high pH (above 13.7), where the stability of ettringite and monosulfate is compromised. The thermodynamic data compiled here allows for the first time to accurately predict the formation and stability of the U-phase in cementitious systems. New information of this nature is vital to assess the physical and chemical durability of different waste management solutions based on cementitious systems for nuclear and industrial waste streams.

ACKNOWLEDGMENTS

The authors acknowledge financial support for this research from the: (a) Electric Power Research Institute (EPRI) and (b) the U.S. Department of Energy's Advanced Research Projects

Agency-Energy (ARPA-e: DE-AR-0001147). This research was conducted in the Laboratory for Chemistry of Construction Materials (LC^2) and the Molecular Instrumentation Center at UCLA. As such, the authors gratefully acknowledge the support that has made these laboratories and their operations possible. The contents of this paper reflect the views and opinions of the authors, who are responsible for the accuracy of the datasets presented herein, and do not reflect the views and/or polices of the agency, nor do the contents constitute a specification, standard or regulation.

REFERENCES

1. Lothenbach B, Kulik DA, Matschei T, Balonis M, Baquerizo L, Dilnesa B, et al. Cemdata18: A chemical thermodynamic database for hydrated Portland cements and alkali-activated materials. Cem Concr Res. 2019 Jan;115:472–506.

2. Ma B, Lothenbach B. Thermodynamic study of cement/rock interactions using experimentally generated solubility data of zeolites. Cem Concr Res. 2020 Sep;135:106149.

3. Matschei T, Lothenbach B, Glasser FP. Thermodynamic properties of Portland cement hydrates in the system $CaO–Al_2O_3–SiO_2–CaSO_4–CaCO_3–H_2O$. Cem Concr Res. 2007 Oct;37(10):1379–410.

4. Lothenbach B, Winnefeld F. Thermodynamic modelling of the hydration of Portland cement. Cem Concr Res. 2006 Feb;36(2):209–26.

5. Lothenbach B, Matschei T, Möschner G, Glasser FP. Thermodynamic modelling of the effect of temperature on the hydration and porosity of Portland cement. Cem Concr Res. 2008 Jan;38(1):1–18.

6. Lothenbach B, Zajac M. Application of thermodynamic modelling to hydrated cements. Cem Concr Res. 2019 Sep;123:105779.

7. Cao Y, Guo L, Chen B, Wu J. Thermodynamic modelling and experimental investigation on chloride binding in cement exposed to chloride and chloride-sulfate solution. Constr Build Mater. 2020 Jun;246:118398.

8. Gin S, Mir AH, Jan A, Delaye JM, Chauvet E, De Puydt Y, et al. A General Mechanism for Gel Layer Formation on Borosilicate Glass under Aqueous Corrosion. J Phys Chem C. 2020 Mar 5;124(9):5132–44.

9. Prentice DP, Walkley B, Bernal SA, Bankhead M, Hayes M, Provis JL. Thermodynamic modelling of BFS-PC cements under temperature conditions relevant to the geological disposal of nuclear wastes. Cem Concr Res. 2019 May;119:21–35.

10. Okoronkwo MU, Balonis M, Katz L, Juenger M, Sant G. A thermodynamics-based approach for examining the suitability of cementitious formulations for solidifying and stabilizing coal-combustion wastes. J Environ Manage. 2018 Jul;217:278–87.

11. Collin M, Prentice DP, Arnold RA, Ellison K, Simonetti DA, Sant GN. Fly Ash–$Ca(OH)_2$ Reactivity in Hypersaline NaCl and $CaCl_2$ Brines. ACS Sustain Chem Eng. 2021 Jun 28;9(25):8561–71.

12. Collin M, Prentice DP, Arnold RA, Ellison K, Simonetti DA, Sant GN. How Brine Composition Affects Fly Ash Reactions: The Influence of (Cat-, An-)ion Type. Adv Civ Eng Mater. 2022 Jun 23;11(2):20210155.

13. Myers RJ, Bernal SA, Provis JL. A thermodynamic model for C-(N-)A-S-H gel: CNASH_ss. Derivation and validation. Cem Concr Res. 2014 Dec;66:27–47.

14. Elakneswaran Y, Owaki E, Miyahara S, Ogino M, Maruya T, Nawa T. Hydration study of slag-blended cement based on thermodynamic considerations. Constr Build Mater. 2016 Oct;124:615–25.

15. Li G, Le Bescop P, Moranville M. The U phase formation in cement-based systems containing high amounts of Na_2SO_4. Cem Concr Res. 1996 Jan;26(1):27–33.

16. Ellison K. Landfill Sequestration of Brine: Research Updates. In: World of Coal Ash. St. Louis, MO; 2019. p. 15.

17. Ellison K. Brine-Encapsulation Bench & Field Testing Recommendations. In: World of Coal Ash. Lexington, KY; 2017. p. 20.

18. Awoyera P, Adesina A. A critical review on application of alkali activated slag as a sustainable composite binder. Case Stud Constr Mater. 2019 Dec;11:e00268.

19. Garcia-Lodeiro I, Palomo A, Fernández-Jiménez A. An overview of the chemistry of alkali-activated cement-based binders. In: Handbook of Alkali-Activated Cements, Mortars and Concretes. Elsevier; 2015. p. 19–47.

20. Dosch W, zur Strassen, H. Ein alkalihaltiges Calciumaluminatsulfathydrat (Natrium-Monosulfat) / An alkali-containing calcium aluminate sulphate hydrate. Zem-Kalk-Gips. 1967;9:11.

21. Christensen AN, Jensen TR, Hanson JC. Formation of ettringite, $Ca_6Al_2(SO_4)_3(OH)_{12}\cdot 26H_2O$, AFt, and monosulfate, $Ca_4Al_2O_6(SO_4)\cdot 14H_2O$, AFm-14, in hydrothermal hydration of Portland cement and of calcium aluminum oxide—calcium sulfate dihydrate mixtures studied by in situ synchrotron X-ray powder diffraction. J Solid State Chem. 2004 Jun;177(6):1944–51.

22. Feng P, Miao C, Bullard JW. Factors Influencing the Stability of AFm and AFt in the Ca-Al-S-O-H System at 25 °C. Riman R, editor. J Am Ceram Soc. 2016 Mar;99(3):1031–41.

23. Matschei T, Lothenbach B, Glasser FP. The AFm phase in Portland cement. Cem Concr Res. 2007 Feb;37(2):118–30.

24. Glasser FP, Kindness A, Stronach SA. Stability and solubility relationships in AFm phases Part I. Chloride, sulfate and hydroxide. Cem Concr Res. 1999;29(6):861–6.

25. Balonis M, Lothenbach B, Le Saout G, Glasser FP. Impact of chloride on the mineralogy of hydrated Portland cement systems. Cem Concr Res. 2010 Jul;40(7):1009–22.

26. Chukanov NV, Britvin SN, Van KV, Mockel S, Zadov AE. Kottenheimite, $Ca_3Si(OH)_6(SO_4)_2.12H_2O$, a new member of the ettringite group from the Eifel area, Germany. Can Mineral. 2012 Feb 1;50(1):55–63.

27. Mesbah A, François M, Cau-dit-Coumes C, Frizon F, Filinchuk Y, Leroux F, et al. Crystal structure of Kuzel's salt $3CaO\cdot Al_2O_3\cdot 1/2CaSO_4\cdot 1/2CaCl_2\cdot 11H_2O$ determined by synchrotron powder diffraction. Cem Concr Res. 2011 May;41(5):504–9.

28. Clark BA, Brown PW. The formation of calcium sulfoaluminate hydrate compounds Part I. Cem Concr Res. 1999;6.

29. Tambara LUD, Cheriaf M, Rocha JC, Palomo A, Fernández-Jiménez A. Effect of alkalis content on calcium sulfoaluminate (CSA) cement hydration. Cem Concr Res. 2020 Feb;128:105953.

30. Li G, Le Bescop P, Moranville M. Expansion mechanism associated with the secondary formation of the U phase in cement-based systems containing high amounts of Na_2SO_4. Cem Concr Res. 1996 Feb;26(2):195–201.

31. Elakneswaran Y, Li C, Kajio T, Owaki E, Ogino M, Nawa T. Durability of slag-blended cement due to U-phase instability in sulphate environment. Mater Struct. 2020 Dec;53(6):146.

32. Lee JK, Chu YS, Kwon CW. The Effects of Alkali Sulfate on the Hydration of a $C_3A-CaSO_4\cdot 2H_2O$ System. J Korean Ceram Soc. 2007 Sep 30;44(9):471–6.

33. Champenois JB, Dhoury M, Cau Dit Coumes C, Mercier C, Revel B, Le Bescop P, et al. Influence of sodium borate on the early age hydration of calcium sulfoaluminate cement. Cem Concr Res. 2015 Apr;70:83–93.

34. Kajio T, et al. Characterization of U-Phase and its prediction in cementitious materials. In: NUWCEM 2018. Avigon; 2018.

35. Chuang L, Kajio T, Owaki E, Morinaga Y, Elakeswaran Y, Nawa T. Sulphate attack in slag-blended cementitious materials hydrated with sodium sulphate. In: Sustainable Construction Materials and Technologies. Kingston University, London, UK; 2019. p. 429–36.

36. Lothenbach B, Gruskovnjak A. Hydration of alkali-activated slag: thermodynamic modelling. Adv Cem Res. 2007 Apr;19(2):81–92.

37. Elakneswaran Y, Owaki E, Nawa T. Modelling Long-Term Durability Performance of Cementitious Materials under Sodium Sulphate Interaction. Appl Sci. 2018 Dec 12;8(12):2597.

38. Borch T, Dionysiou D, Katz L, Xu P, Breckenridge R, Ellison K, et al. National Alliance for Water Innovation (NAWI) Technology Roadmap: Agriculture Sector. 2021.

39. Cath T, Chellam S, Katz L, Breckenridge R, Cooper CA, Ellison K, et al. National Alliance for Water Innovation (NAWI) Technology Roadmap: Resource Extraction Sector. 2021.

40. Cath T, Chellam S, Katz L, Kim J, Breckenridge R, Macknick J, et al. National Alliance for Water Innovation (NAWI) Technology Roadmap: Industrial Sector. 2021.

41. Childress A, Giammar D, Jiang S, Macknick J, Plata S, Sedlak D, et al. National Alliance for Water Innovation (NAWI) Technology Roadmap: Power Sector. 2021.

42. Giammar D, Jiang S, Xu P, Breckenridge R, Edirisooriya T, Jiang W, et al. National Alliance for Water Innovation (NAWI) Technology Roadmap: Municipal Sector. 2021.

43. Li G. Etude du phénomène de l'expansion sulfatique dans les bétons: comportement des enrobés de déchets radioactifs sulfatés [physics.med-ph]. Ecole Nationale des Ponts et Chaussées; 1994.

44. Li G, Le Bescop P, Moranville-Regourd M. Synthesis of the U phase ($4CaO{\cdot}0.9Al_2O_3{\cdot}1.1SO_3{\cdot}0.5Na_2O{\cdot}16H_2O$). Cem Concr Res. 1997 Jan;27(1):7–13.

45. Lothenbach B, Durdziński PT, De Weerdt K. Thermogravimetric analysis. In: A practical guide to Microstructural analysis of cementitious materials. Boca Raton; 2016.

46. Shi Z, Geiker MR, Lothenbach B, De Weerdt K, Garzón SF, Enemark-Rasmussen K, et al. Friedel's salt profiles from thermogravimetric analysis and thermodynamic modelling of Portland cement-based mortars exposed to sodium chloride solution. Cem Concr Compos. 2017 Apr;78:73–83.

47. Laugier J, Bochu B. LMGP-Suite Suite of Programs for the interpretation of X-ray Experiments [Internet]. BP 46. 38042 Saint Martin d'Hères, France: ENSP/Laboratoire des

Matériaux et du Génie Physique; Available from: http://www.inpg.fr/LMGP and http://www.ccp14.ac.uk/tutorial/lmgp/

48. Kulik DA, Wagner T, Dmytrieva SV, Kosakowski G, Hingerl FF, Chudnenko KV, et al. GEM-Selektor geochemical modeling package: revised algorithm and GEMS3K numerical kernel for coupled simulation codes. Comput Geosci. 2012 Aug 24;

49. Wagner T, Kulik DA, Hingerl FF, Dmytrieva SV. GEM-Selektor geochemical modeling package: TSolMod library and data interface for multicomponent phase models. Can Mineral. 2012 Oct 1;50(5):1173–95.

50. Thoenen T, Hummel W, Berner U, Curti E. The PSINagra chemical thermodynamic database 12/07. Villigen PSI. Switzerland; 2014.

51. Hummel W, Berner U, Curti E, Pearson FJ, Thoenen T. Nagra/PSI Chemical Thermodynamic Data Base 01/01. Radiochim Acta. 2002 Jan 1;90(9–11).

52. Johnson JW, Oelkers EH, Helgeson HC. SUPCRT92: A software package for calculating the standard molal thermodynamic properties of minerals, gases, aqueous species, and reactions from 1 to 5000 bar and 0 to 1000 °C. Comput Geosci. 1992 Aug;18(7):899–947.

53. Helgeson HC, Kirkham DH, Flowers GC. Theoretical prediction of the thermodynamic behavior of aqueous electrolytes by high pressures and temperatures; IV, Calculation of activity coefficients, osmotic coefficients, and apparent molal and standard and relative partial molal properties to 600 °C and 5 kb. Am J Sci. 1981;281(10):1249–516.

54. Vollpracht A, Lothenbach B, Snellings R, Haufe J. The pore solution of blended cements: a review. Mater Struct. 2016 Aug;49(8):3341–67.

55. Horgnies M, Chen JJ, Bouillon C. Overview about the use of Fourier Transform Infrared spectroscopy to study cementitious materials. In: Materials Characterisation VI. Siena, Italy; 2013. p. 251–62.

56. Gastaldi D, Canonico F, Boccaleri E. Ettringite and calcium sulfoaluminate cement: investigation of water content by near-infrared spectroscopy. J Mater Sci. 2009 Nov;44(21):5788–94.

57. Baquerizo LG, Matschei T, Scrivener KL, Saeidpour M, Wadsö L. Hydration states of AFm cement phases. Cem Concr Res. 2015 Jul;73:143–57.

58. Sánchez-Herrero MJ, Fernández-Jiménez A, Palomo A. C4A3Š hydration in different alkaline media. Cem Concr Res. 2013 Apr;46:41–9.

59. Walker TM, Howitt DG. Field-Induced Migration of Sodium in Soda Silicate Glasses During Scanning Electron Microscopy. Scanning. 1989;11(5–11).

60. Balonis M, Glasser FP. The density of cement phases. Cem Concr Res. 2009 Sep;39(9):733–9.

61. Rojas MF, Cabrera J. The effect of temperature on the hydration rate and stability of the hydration phases of metakaolin–lime–water systems. Cem Concr Res. 2002 Jan;32(1):133–8.

62. Damidot D, Lothenbach B, Herfort D, Glasser FP. Thermodynamics and cement science. Cem Concr Res. 2011 Jul;41(7):679–95.

63. Lothenbach B. Thermodynamic equilibrium calculations in cementitious systems. Mater Struct. 2010 Dec;43(10):1413–33.

64. Shock EL, Sassani DC, Willis M, Sverjensky DA. Inorganic species in geologic fluids: Correlations among standard molal thermodynamic properties of aqueous ions and hydroxide complexes. Geochim Cosmochim Acta. 1997 Mar;61(5):907–50.

65. Robie RA, Hemingway BS. Thermodynamic properties of minerals and related substances at 298.15 K and 1 bar (10^5 pascals) pressure and at higher temperatures. 1995. (Bulletin). Report No.: 2131.

66. Kondepudi D, Prigogine I. Modern Thermodynamics: From Heat Engines to Dissipative Structures. 1st ed. Wiley; 2014.

67. Chase MW, National Institute of Standards and Technology (U.S.), editors. NIST-JANAF thermochemical tables. 4th ed. Washington, DC : New York: American Chemical Society ; American Institute of Physics for the National Institute of Standards and Technology; 1998. 2 p.

68. Lange NA. Lange's handbook of chemistry. 12. ed. Dean JA, editor. New York: McGraw-Hill; 1979.

69. Helgeson HC, Delany J, Nesbitt HW, Bird DK. Summary and critique of the thermodynamic properties of rock forming minerals. Am J Sci. 1978;278-A.

70. Lothenbach B, Pelletier-Chaignat L, Winnefeld F. Stability in the system $CaO–Al_2O_3–H_2O$. Cem Concr Res. 2012 Dec;42(12):1621–34.

71. Zhen-Wu BY, Prentice DP, Ryan JV, Ellison K, Bauchy M, Sant G. zeo19: A thermodynamic database for assessing zeolite stability during the corrosion of nuclear waste immobilization glasses. Npj Mater Degrad. 2020 Dec;4(1):2.

72. Glasser L. The effective volumes of waters of crystallization & the thermodynamics of cementitious materials. Cement. 2021 Mar;3:100004.

73. Ghazizadeh S, Hanein T, Provis JL, Matschei T. Estimation of standard molar entropy of cement hydrates and clinker minerals. Cem Concr Res. 2020 Oct;136:106188.

74. Parrot LJ, Killoh DC. Prediction of cement hydration. Proc Br Ceram Soc. 1984;35:41–53.

75. Taylor HFW. Cement chemistry. 2nd ed. 1997.

76. Prentice DP, Bernal SA, Bankhead M, Hayes M, Provis JL. Phase evolution of slag-rich cementitious grouts for immobilisation of nuclear wastes. Adv Cem Res. 2018 Sep;30(8):345–60.

Prepared for Submission to Journal of the American Ceramic Society (April 2023)

Solubility behavior and thermodynamic modeling of sodium monosulfoaluminate ("U-phase") in cementitious systems

Marie Collin ([1,2]), Dale P. Prentice ([1,2]), Ross R. Arnold ([1,2]), Kirk Ellison ([3]), Magdalena Balonis ([4]), Dante Simonetti ([2,5]), Gaurav N. Sant ([1,2,4,6])

Supplementary information

6 Pages

2 Figures

2 Tables

[1] Laboratory for the Chemistry of Construction Materials (LC^2), Department of Civil and Environmental Engineering, University of California, Los Angeles, CA, USA

[2] Institute for Carbon Management, University of California, Los Angeles, CA, USA

[3] Electric Power Research Institute, Charlotte, NC 28262, USA

[4] Department of Materials Science and Engineering, University of California, Los Angeles, CA, USA

[5] Department of Chemical and Biomolecular Engineering, University of California, Los Angeles, CA, USA

[6] California Nanosystems Institute (CNSI), University of California, Los Angeles, CA, USA

Corresponding authors: M. Collin (mariecollin03@ucla.edu) and G. Sant (Email: gsant@ucla.edu)

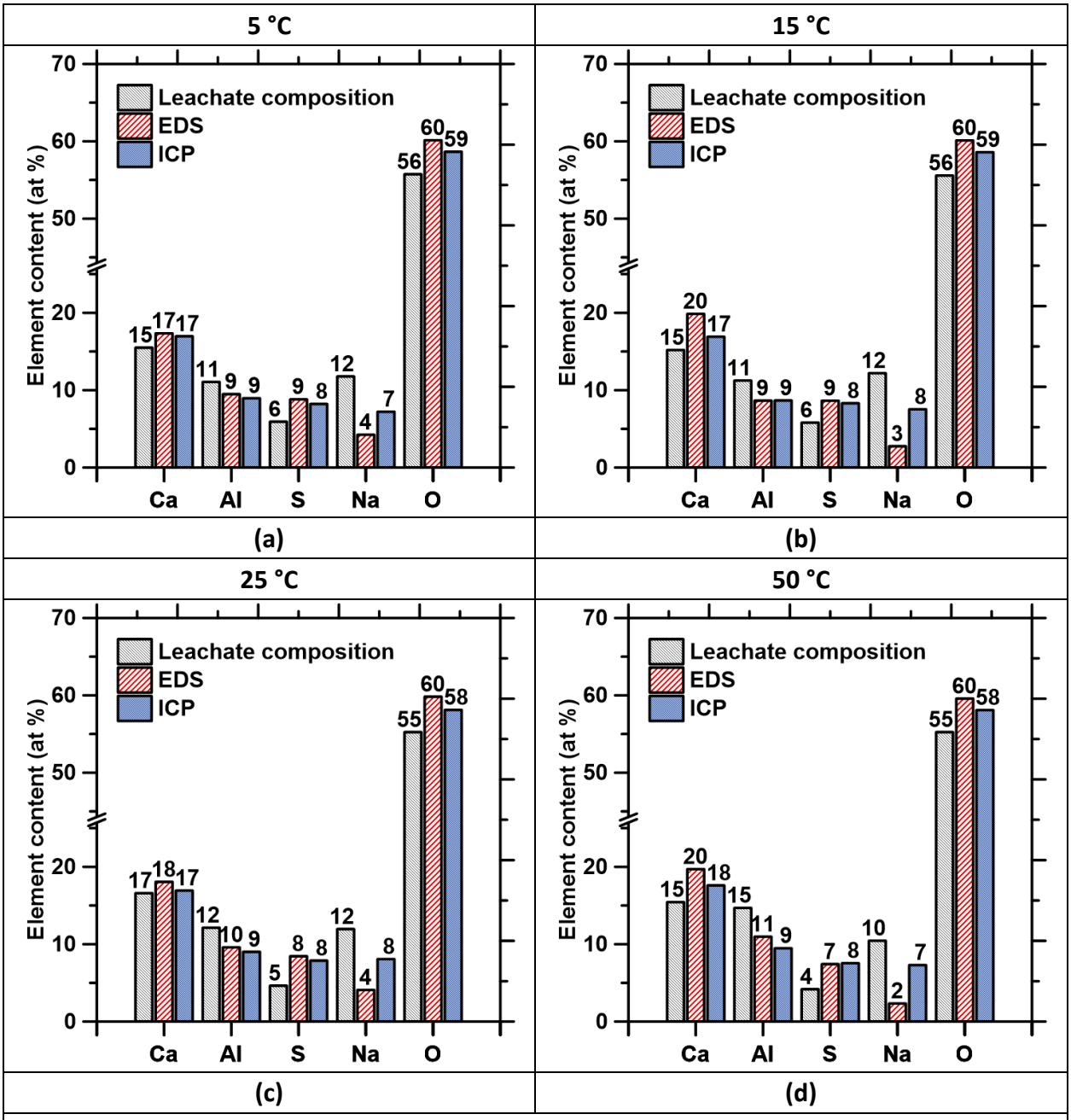

Figure S1. A comparison between the average solid composition as determined from the mass balance of the "mother liquor" from which the solid forms, SEM-EDS analysis, and solid digestion for samples synthesized at **(a)** 5, **(b)** 15, **(c)** 25 and **(d)** 50 °C.

Table S1. The solution composition of the synthesis solutions at: 5, 15, 25, and 50 °C. The symbol * indicates outlier values. The bolded log K_{so} values were chosen for the average value calculation.

Temperature (°C)	[Al] (mmol/L)	[Ca] (mmol/L)	[SO_4^{2-}] (mmol/L)	[Na] (mmol/L)	pH	Log K_{so}
5	460	5.20*	289	1650	$pH_{5\,°C}$ = 14.00	-21.17
	464	3.65	355	1648	$pH_{5\,°C}$ = 14.00	**-21.73**
	448	3.64	284	1582	$pH_{5\,°C}$ = 14.00	**-21.87**
					Average =	**-21.80**
15	448	2.47	332	1596	$pH_{15\,°C}$ = 13.85	**-21.83**
	442	14.30*	296	1632	$pH_{15\,°C}$ = 13.85	-18.78
	448	2.73	305	1598	$pH_{15\,°C}$ = 13.85	**-21.66**
					Average =	**-21.75**
25	442	3.01	458*	1666	$pH_{25\,°C}$ = 13.64	-21.34
	452	2.53	288	1626	$pH_{25\,°C}$ = 13.64	**-21.79**
	452	4.04*	314	1642	$pH_{25\,°C}$ = 13.64	-20.93
					Average =	**-21.79**
50	346	8.24*	390	1668	$pH_{50\,°C}$ = 13.22	-20.59
	332	3.24	329	1636	$pH_{50\,°C}$ = 13.22	**-22.35**
	342	3.42	376	1702	$pH_{50\,°C}$ = 13.22	**-22.13**
					Average =	**-22.24**

Table S2. Thermodynamic properties of the solid and aqueous constituents used to calculate $\Delta_f G^\circ_{298}$, $\Delta_f H^\circ_{298}$, $\Delta_f S^\circ_{298}$ and Cp°_{298} for the U-phase. Reference state of 298.15 K and 1 bar.

Species	$\Delta_f \boldsymbol{G^\circ_{298}}$	$\Delta_f \boldsymbol{H^\circ_{298}}$	$\boldsymbol{S^\circ_{298}}$	$\boldsymbol{Cp^\circ_{298}}$	**Ref**
	(kJ/mol)	(kJ/mol)	(J/mol)	(J/mol/K)	
Solids					
Monosulfate – $Ca_4Al_2(SO_4)(OH)_{12}\cdot 6H_2O$	-7778.4	-8758.6	791.6	948.4	(1)
Thenardite – Na_2SO_4	-379.6	-425.8	64.4	59.5	(2)
Aqueous constituents					
Ca^{2+}	-552.79	-543.07	-56.48	-30.92	(3)
Na^{+}	-261.88	-240.28	58.41	38.12	(3)
AlO_2^{-}	-827.48	-925.57	-30.21	-49.04	(3)
OH^{-}	-157.27	-230.01	-10.71	-136.34	(3)
SO_4^{2-}	-744.46	-909.70	18.83	-266.09	(3)
$H_2O°$	-237.18	-285.88	69.92	75.36	(4)

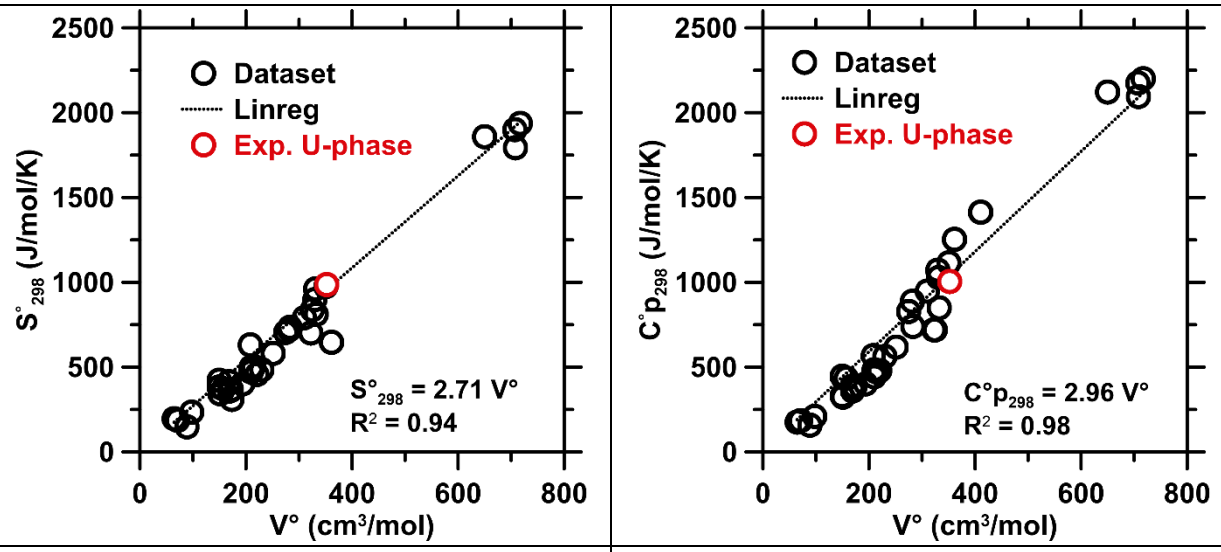

Figure S2. A comparison between the thermodynamic properties of the U-phase, and that of calcium silicate mineral hydrates from the slop98.dat, Cemdata18, and Zeo19 thermodynamic databases(4–9) showing comparisons for: **(a)** Entropy (S°_{298}), and **(b)** Heat capacity ($C^{\circ}p_{298}$) as a function of the molar volume V° (i.e., following the volume-based thermodynamics approach).(10,11)

REFERENCES

1. Baquerizo LG, Matschei T, Scrivener KL, Saeidpour M, Wadsö L. Hydration states of AFm cement phases. Cem Concr Res. 2015 Jul;73:143–57.

2. Robie RA, Hemingway BS. Thermodynamic properties of minerals and related substances at 298.15 K and 1 bar (10^5 pascals) pressure and at higher temperatures [Internet]. 1995. (Bulletin). Report No.: 2131. Available from: http://pubs.er.usgs.gov/publication/b2131

3. Shock EL, Sassani DC, Willis M, Sverjensky DA. Inorganic species in geologic fluids: Correlations among standard molal thermodynamic properties of aqueous ions and hydroxide complexes. Geochim Cosmochim Acta. 1997 Mar;61(5):907–50.

4. Johnson JW, Oelkers EH, Helgeson HC. SUPCRT92: A software package for calculating the standard molal thermodynamic properties of minerals, gases, aqueous species, and reactions from 1 to 5000 bar and 0 to 1000 °C. Comput Geosci. 1992 Aug;18(7):899–947.

5. Lothenbach B, Matschei T, Möschner G, Glasser FP. Thermodynamic modelling of the effect of temperature on the hydration and porosity of Portland cement. Cem Concr Res. 2008 Jan;38(1):1–18.

6. Lothenbach B, Kulik DA, Matschei T, Balonis M, Baquerizo L, Dilnesa B, et al. Cemdata18: A chemical thermodynamic database for hydrated Portland cements and alkali-activated materials. Cem Concr Res. 2019 Jan;115:472–506.

7. Thoenen T, Hummel W, Berner U, Curti E. The PSINagra chemical thermodynamic database 12/07. Villigen PSI. Switzerland; 2014.

8. Hummel W, Berner U, Curti E, Pearson FJ, Thoenen T. Nagra/PSI Chemical Thermodynamic Data Base 01/01. Radiochim Acta [Internet]. 2002 Jan 1 [cited 2021 Jan 13];90(9–11). Available from: http://www.degruyter.com/view/j/ract.2002.90.issue-9-11/ract.2002.90.9-11_2002.805/ract.2002.90.9-11_2002.805.xml

9. Zhen-Wu BY, Prentice DP, Ryan JV, Ellison K, Bauchy M, Sant G. zeo19: A thermodynamic database for assessing zeolite stability during the corrosion of nuclear waste immobilization glasses. Npj Mater Degrad. 2020 Dec;4(1):2.

10. Glasser L. The effective volumes of waters of crystallization & the thermodynamics of cementitious materials. Cement. 2021 Mar;3:100004.

11. Ghazizadeh S, Hanein T, Provis JL, Matschei T. Estimation of standard molar entropy of cement hydrates and clinker minerals. Cem Concr Res. 2020 Oct;136:106188.